Lattice model for the kinetics of rupture of fluid bilayer membranes

Luc Fournier and Béla Joós*
Ottawa Carleton Institute of Physics, University of Ottawa Campus, Ottawa, Ontario, Canada K1N-6N5
(Received 15 March 2002; revised manuscript received 18 February 2003; published 14 May 2003)

We have constructed a model for the kinetics of rupture of membranes under tension, applying physical principles relevant to lipid bilayers held together by hydrophobic interactions. The membrane is characterized by the bulk compressibility (for expansion) K, the thickness $2h_t$ of the hydrophobic part of the bilayer, the hydrophobicity σ, and a parameter γ characterizing the tail rigidity of the lipids. The model is a lattice model which incorporates strain relaxation, and considers the nucleation of pores at constant area, constant temperature, and constant particle number. The particle number is conserved by allowing multiple occupancy of the sites. An equilibrium ''phase diagram'' is constructed as a function of temperature and strain with the total pore surface and distribution as the order parameters. A first-order rupture line is found with increasing tension, and a continuous increase in protopore concentration with rising temperature till instability. The model explains current results on saturated and unsaturated phosphatidylcholine lipid bilayers and thicker artificial bilayers made of diblock copolymers. Pore size distributions are presented for various values of area expansion and temperature, and the fractal dimension of the pore edge is evaluated.

DOI: 10.1103/PhysRevE.67.051908 PACS number(s): 87.16.Dg, 87.16.Ac, 87.14.Cc, 68.60.Dv

I. INTRODUCTION

Fluid bilayer membranes made of lipids separate the contents of cells from their surroundings. The stability of those membranes under external perturbations is consequently of vital importance. In particular, if ruptured the functions of the cell will be disabled. Naturally, a red cell bilayer membrane may rupture to free hemoglobin, protein responsible for oxygen transportation in blood. This particular rupture, called blood cell hemolysis is achieved through thermal swelling of red cells [1]. Rupture or lysis can be achieved in a number of ways. Most experiments involved application of electric fields that produce compressive forces through the capacitor effect [2–7]. More recently a number of other ways have been used: mechanically, by suction through a pipette [8] or extrusion through pores [9]; and by osmotic swelling of the cell [10–12]. With the rapid progress in microscopic manipulation techniques, pore formation can also serve a positive purpose in drug delivery and gene therapy [13–15]. The number of experimental studies of the mechanical properties of the cell is rapidly increasing and we only quoted a few examples of recent work [16].

For the fluid bilayers, there is a significant degree of consensus on the order of magnitude of the quantities involved in membrane rupture. For phosphatidylcholine (PC) bilayers, area expansion seems to be only 2%–4% before rupture. The corresponding external tension is of the order of 10^{-3}–10^{-2} N/m [4,8,17–19]. It also seems that in liquid membranes, rupture occurs via the nucleation of holes. Those observations are consistent with what is expected from structural considerations. Solid membranes as they go from brittle to ductile, experience rupture kinetics that evolve from processes dominated by crack formation to hole formation [20]. More precisely, as the surface tension increases, the membrane will first be weakened by the apparition of small unstable pores with lifetimes as short as a few nanoseconds. At a critical tension, a large stable pore opens, relaxing almost entirely the membrane. This is rupture. Pore sizes can range from nanometer to micrometer in radius. In electroporation experiments, pores can last several microseconds [2–5,21]. Using mechanical means, namely, micropipette extrusion on vesicles, pores can be kept open for several seconds before resealing [22,23].

Several models of membrane rupture have been developed over the years. Most of them derive from a model suggested by Litster a quarter of a century ago [24]. It explains the stability in terms of a surface energy and a pore edge energy. The model defines a critical pore size and an energy barrier for the creation of an irreversibly growing pore. It has been extended and applied by other groups, in particular, to electric breakdown situations [3,25,26]. Shillcock and Boal investigated the effect of temperature on membrane stability [27]. Temperature increases the entropy of the pore lowering its free energy. They show that even at zero tension, edge energy is required for stability. Netz and Schick have also developed a mean-field theory of the fluid bilayers as stacks of diblock copolymers [28].

In our work, we derive the energy of a finite size membrane under lateral expansion. We then consider pore creation as a thermally activated process [29]. There is an important entropic element implied in a nucleation process. The model is for a bilayer whose relevant physical quantities have their origin in the hydrophobicity of the lipid tails [31,32]. These quantities are the area compressibility (for expansion) K, which results from the increased exposure of the hydrophobic tails as the membrane is stretched, the edge tension λ (or edge energy per unit length), which is the result of the exposure of these tails to water along the edge of the pore, and the rigidity γ of the tails.

In the model, the bilayer is characterized by an energy per site, essentially one molecule in size. It incorporates stress relaxation as a pore is created and grows. Pore-pore interactions are automatically taken into account. An equilibrium phase diagram is constructed as a function of the temperature and the area expansion of the membrane. The critical tem-

*Electronic address: bjoos@uottawa.ca

peratures scale with the strength of the hydrophobic interaction which to first order is linked to the length of the tails of the lipids. This hydrophobic interaction is obtained from parameters appropriate for pure PC [8,19]. Our model applies to low strain rates since the model assumes that the membrane remains in mechanical equilibrium as it is stretched. We predict the rupture scenario for normal membranes, membranes made of unsaturated lipids, and very thick membranes.

The following two sections develop the model. We first lay its physical foundations, and then present our Ising-like model, which is solved using Monte Carlo simulations. We continue with the results and finish with a discussion of the possible extensions of the model.

II. MODEL FOR MEMBRANE RUPTURE

Upon area increase, stress will buildup in the membrane. As mentioned earlier, being a liquid the most likely stress release mechanism will be the formation of holes or pores. Let us imagine that a hole has appeared through thermal induced stress fluctuations. The question will be whether the gain in energy occasioned by the relaxation of the surfactants will counterbalance the energy loss through exposure of the tails of the molecule to the solvent. If this is the case, the hole will continue to grow into a large pore that will permit the system to relax almost entirely. For now, we assume the process to be purely planar. Whether fluctuations in the third dimension are important is an open question. At first thought they do not seem predominant. Assuming an elastic regime for small expansions of the membrane on a lattice of total relaxed area a_m and molecular area a_0, the energy cost associated with the stretching of the membrane is given by

$$E_m = \frac{1}{2} K a_m \left(\frac{\Delta a}{a_0} \right)^2, \tag{1}$$

where K is the compressibility (for expansion) and $\Delta a = a - a_0$ the excess area per molecule. For small expansion, the compressibility can be found experimentally from various techniques described previously. The apparent compressibility is the measure of the slope of the stress-strain curve of a membrane under a small tension, that is, the slope of the curve

$$\tau = K \left(\frac{\Delta a}{a_0} \right), \tag{2}$$

where τ is the surface tension. However, since those membranes are fluid, thermal transverse undulations are usually present. For small stretches, a fraction of the tension does not induce any strain, but rather brings back the membrane in its plane [33]. The real compressibility is obtained by the slope of the stress-strain curve, but only in the regime where the undulations have been ironed out. For many lipids, this compressibility is about 243 mN/m [19].

When a single pore is inserted, some of this stress will be relieved. The relative change in the area per molecule becomes

$$\frac{\Delta a}{a_0} = \frac{\Delta a_m}{a_m} - \frac{a_p}{a_m}, \tag{3}$$

where a_p is the area of the pore and Δa_m is the total expansion of the membrane. But the edge of the new pore will now be exposed to water. As the tails are hydrophobic, this will result in an increase of the energy proportional to the perimeter of the pore. For simplicity, we will assume the pore to be circular. In the presence of a pore, the energy of a stretched membrane then becomes

$$E_m(a_p) = 2\lambda \sqrt{\pi a_m} \left(\frac{a_p}{a_m} \right)^{1/2} + \frac{1}{2} K a_m \left(\frac{\Delta a}{a_0} \right)^2. \tag{4}$$

The parameter λ represents the edge tension (the effective edge energy per unit length). The first term in Eq. (4) is the total edge energy, which represents the loss of energy on the perimeter of the circular hole. The second term, the surface energy, is the loss in energy resulting from the relaxation of the membrane induced by the hole, which augments the density of particles in the rest of the membrane. For the edge tension, it can be rewritten as

$$\lambda = 2 h_t \sigma, \tag{5}$$

where $2h_t$ is the hydrophobic thickness of the bilayer, and therefore h_t is the length of the lipid tails. And σ, the hydrophobicity, is the hydrophobic energy of the lipid tails per unit area. With the usually quoted hydrophobicity of about 40 mN/m [31,32], the edge tension λ is of the order of 10^{-7} mN [22,32]. The experimentally measured values range from 1 to 4×10^{-8} mN [22].

In the limit of large systems, the energy barrier to rupture is given by $\lambda^2 \pi / K (\Delta a_m / a_m)^{-1}$ and occurs for a pore area $a_p = (\lambda a_m \sqrt{\pi}/K)^{2/3}$. When a_p exceeds that critical value, the pore will grow till the membrane reaches the minimum energy configuration near $a_p = \Delta a_m$. This argument predicts a barrier height of the order of $10^4 k_B T_{room}$ ($k_B T_{room} = 4.14 \times 10^{-18}$ mJ) for experimentally observed stretches, such as $\Delta a_m / a_m = 4\%$ and a membrane of total area 1 μm^2, typical for PC membranes. Even if the entropic components were very significant as mentioned above, it is not sufficient to decrease significantly this large barrier. Moreover, according to these arguments, rupture should only happen at stretches around $\Delta a_m / a_m = 50\%$.

In our opinion, the problem lies in an overestimation of the line energy due to two factors. First, when membranes expand, the tails get exposed to water, so h_t is not a constant (especially not at 50%) . It decreases with increased stretching of the membrane. Second lipid bilayers are permeable and this permeability may be affected by the expansion of the membrane. So the hydrophobicity σ used in the computation of the line energy will be smaller than the ideal value quoted above. We call σ an *apparent* hydrophobicity and the σ given above the *pure* hydrophobicity σ_{pure}. σ will be an adjustable parameter.

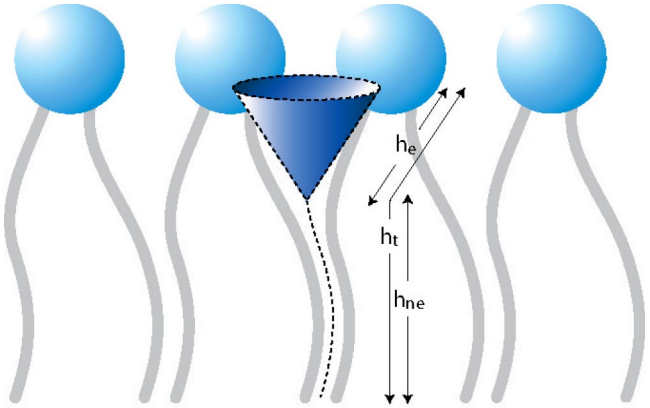

FIG. 1. (Color online only) Schematic representation of the total height of the lipid tails exposed to water at a given expansion. The rigidity γ is the ratio of surface of the sides of the cones to the base. The total surface exposed to water is expected to be larger than the surface expansion.

Compressibility, hydrophobicity, and tail rigidity

Under expansion, more water will enter the membrane, augmenting the free energy. The compressibility (upon expansion) K has therefore its origin in hydrophobicity. Moreover, the rigidity of the acyl tails controls the amount of water that penetrates the membrane at a given stretch. There is therefore a very close relationship between surface energy, compressibility and tail rigidity. We will closely follow here some of the arguments of Wortis and Evans [32] (themselves based partly on Israelachvili's book [31]) for what pertains to the compressibility but adding the concept of the rigidity of the tails.

To estimate K, we must understand the balance of forces that sets the area of the lipids a. The repulsive force between lipids is strong at short distances, but falls off rapidly as a increases [32]. This repulsion is modeled by a potential of the form D/a, where D is a positive constant. On the other hand, the attractive part of the potential is a direct consequence of hydrophobicity. More water can enter in contact with the hydrocarbon chains as the lipids are separated from one another. In an earlier work [31,32], a linear regime is assumed for small expansions of the cross section area of a lipid a, and the energy per molecule is written as $\sigma(a-a_0)$, where a_0 is the equilibrium area. This assumes that the tails are totally flexible and that the area exposed to water is equal to the increase in area of the membrane $(a-a_0)$. However, as illustrated in Fig. 1, the lipid tails more likely will only be able to partially close up the opening. We introduce a geometrical factor $\gamma>1$, defined so that $\gamma(a-a_0)$ represents the actual surface exposed to water per molecule under stretching, and hence $\sigma\gamma(a-a_0)$ the increased energy per molecule. The factor γ is related to the rigidity of the tails, and therefore from now on γ will be referred as the tail rigidity. To have a geometric picture of γ, let us imagine that the stretching Δa is represented by a circle, and the effective exposed surface by a cone of surface S, as shown in Fig. 1. γ is then the ratio $S/\Delta a$. A rigidity of one represents tails that are completely flexible since the expanded lateral surface Δa is equal to the increased exposure of the tails to water. In contrast, a high rigidity represents very stiff chains, such that a small stretch can lead to a full exposure of the tails to water. With the geometry shown in Fig. 1, the length h_e of the tails exposed to water can be written as

$$h_e=\gamma r\left(\frac{\Delta a}{a_0}\right)^{1/2}, \tag{6}$$

where $r=\sqrt{a/\pi}$ is the radius of the lipids. The nonexposed length $h_{ne}=h_t-h_e$ should be used in Eq. (5) to calculate the line energy when a pore is nucleated at a certain stretch. Fixing the rigidity γ for a certain type of lipid determines h_e and h_{ne} as a function of the effective stretch.

If we combine both the attractive and the repulsive parts of the potential, we get a general expression for the energy per molecular site of the membrane:

$$U(a)=2\sigma\gamma(a-a_0)+D(a^{-1})+U_0. \tag{7}$$

The factor of 2 in the first term comes from the fact that we are dealing with a bilayer. The requirement $dU/da|_{a_0}=0$ leads to the relationship $D=2\sigma\gamma a_0^2$. It must be emphasized that σ here represents the interaction of the lipids when present in the membrane, and therefore refers to the *apparent* hydrophobicity, in opposition to the pure hydrophobicity σ_{pure} discussed earlier in this section. By comparing the curvature of this potential around the minimum with the surface energy of Eq. (1), we obtain

$$K=4\sigma\gamma. \tag{8}$$

Thus, there is a close relationship between the compressibility K, the hydrophobicity σ, and the rigidity γ. In our simulations, we use the experimentally known values of compressibility K, and set the rigidity γ to obtain rupture near 4% for the PC-type bilayers. With the use of Eq. (8), we shall demonstrate in Sec. IV B that the apparent hydrophobicity σ is considerably smaller than the pure one σ_{pure}, which ignores the water already present in the membrane. With σ_{pure} the line energy is overestimated as we saw above.

III. THE CALCULATION

What we are trying to simulate is a thermally activated nucleation process, it is therefore natural to consider a model amenable to a Monte Carlo simulation. For ease of computation, we consider a lattice model similar to the well-known Ising model for binary mixtures, and consider the equilibrium phase diagram of the system as a function of temperature and area expansion. This will reveal the expected scenarios of rupture as the membrane is expanded slowly, quasistatically, so that the membrane remains in thermodynamic equilibrium at every step of the way. We will limit ourselves to two dimensions, and to represent an isotropic liquid, we will use a hexagonal lattice (six nearest neighbors). We begin by presenting the standard binary mixture model (SBMM) as applied to our problem and then describe the modifications and simplifications that we have made to it to incorporate the stress relaxation that occurs when a hole is created. In the SBMM, every site can be in

either of two states, in our case "a" or "h," representing, respectively, sites occupied by a phospholipid or a hole. The site occupancy variable s_i, is equal to 1 if the site is an "a" site and 0 if it is an "h" site. The indices i and j run from 1 to N, where N is the total number of sites. Let $J_{aa}(r_{ij})$, or its compact form J_{ij}^{aa}, be the interaction between two lipids separated by a distance $r_{ij}=|\mathbf{R}_i-\mathbf{R}_j|$, where $\mathbf{R}_i$ is the position vector for site i. In a similar way, $J^{hh}(r_{ij})$ and $J^{ah}(r_{ij})$ are defined. The microscopic Hamiltonian H consists of the sum of all interactions:

$$H=\frac{1}{2}\sum_{ij}\{J_{ij}^{aa}s_is_j+J_{ij}^{hh}(1-s_i)(1-s_j)+J_{ij}^{ah}[s_i(1-s_j)+s_j(1-s_i)]\}. \tag{9}$$

In a conventional canonical binary mixture, one would expand Eq. (9) and eliminate the constant terms and the single sums since the number of each type of particle is conserved. In our binary mixture model, we keep the number N of particles (the a sites) and the total area constant. The number of holes (the h sites), however, can vary. Our model is neither the conventional canonical nor grand canonical version of the binary mixture model. In the canonical ensemble, occupied (a) and empty (h) sites are interchanged to preserve the total number of particles. The conventional canonical model would be used if we were only interested in the phase separation of a system, which is not our case. In the grand canonical ensemble, the only dynamics that would be observed is the distribution of the holes. Neither model is suitable to incorporate the relaxation created by the appearance of a hole.

We start with the SBMM in the canonical ensemble with an initial total number of particles equal to the number of sites N. We now modify the model to impose the following constraints: the total area of the membrane stays constant as holes are created and the total number of lipids—a particles—stays constant. These lead to the following change in the dynamics. Occupied sites, when holes are created, now contain more than one particle, actually $N/(N-n_h)$, where n_h is the number of hole sites at a given time. The area of the occupied and hole sites stay constant. The nucleation of holes therefore relaxes the membrane and reduces the interparticle distance r_{ij}. This relaxation represents the surface energy and is the J_{ij}^{aa} term in Eq. (9).

On the other hand, the interaction energy between holes and particles J_{ij}^{ah} represents the line energy of pores. The occupancy of sites being larger than one in such a case, there are more particles on the edge than the actual number of sites. As we will discuss in Sec. III B, this will lead to a correction in the line energy. Finally, the hole-hole interaction J_{ij}^{hh} is set to zero.

A. The surface energy

The surface energy is not calculated using the first term in Eq. (9) but directly using the occupied area in the membrane. With n_h hole sites, the interparticle distances have to be rescaled to the new values

$$\tilde{r}_{ij}=\left(\frac{N-n_h}{N}\right)^{1/2}r_{ij}, \tag{10}$$

where the $r_{ij}=|\mathbf{R}_i-\mathbf{R}_j|$ are the initial intermolecular distances. As discussed earlier, the nucleation of holes changes the density of lipids in the membrane but conserves their number. Since we assume uniform relaxation at each step of the simulation, the relative change in area per lipid, defined in Eq. (3), can be rewritten as

$$\frac{\Delta a}{a_0}=\frac{\Delta a_m}{a_m}-\frac{a_p}{a_m}=\frac{\Delta a_m}{a_m}-\frac{n_h}{N}, \tag{11}$$

where a_p is now the total pore area, and not just the area of one pore. The surface energy can be calculated directly using the compressibility from the relation,

$$E_s=\frac{1}{2}Ka_m\left(\frac{\Delta a}{a_0}\right)^2. \tag{12}$$

It is clear from this last equation that if the relative number of holes n_h/N completely relaxes the imposed stretch on the membrane $\Delta a_m/a_m$, the surface energy vanishes, as expected.

B. The line energy

As previously mentioned, the line (or edge) energy represents the hydrophobic contacts along the perimeter of a pore, measured by the hole-lipid interaction J_{ij}^{ah}. The edge energy therefore depends on the location of the holes in the lattice. The sum of those interactions cannot be reduced to a simple form like the surface energy.

As we are working on a hexagonal lattice, J_{ij}^{ah} consists of the energy of exposing one-sixth of the hydrophobic surface of a lipid to water, multiplied by 2 for the bilayer. It is a first neighbor interaction. J_{ij}^{ah} can be written as

$$J_{ij}^{ah}=J^{ah}=\begin{cases}\frac{2}{3}h_{ne}\sigma\sqrt{\pi a_0} & \text{if } r_{ij} \text{ is 1st neighbor}\\ 0 & \text{otherwise,}\end{cases} \tag{13}$$

where a_0 is the cross section of the lipids and $h_{ne}=h_t-h_e$ the hydrophobic length of the lipid tails that are not exposed to water [h_t and h_e are defined in Eqs. (5) and (6), respectively]. The hydrophobic energy of the exposed height h_e is the origin of the surface energy.

In the simulation the occupancy variables s_i remain equal to either 0 or 1. So the edge energy as calculated by the program is

$$E_{edge}^{\text{model}}=J^{ah}L^{ah}, \tag{14}$$

where L^{ah} is the number of lipid-hole interactions (between sites).

However, every time a hole site is created, the density of the particles and hence the interparticle distance changes as expressed in Eq. (10), in particular, the nearest neighbor in-

terparticle distance r . There are, therefore, more particles on the edge of a pore than the actual number of sites. The edge energy per unit length can be written as $J^{ah}/\tilde{r}$, where $\tilde{r}$ is the scaled nearest neighbor interparticle distance. And hence, the correct expression for the line energy is

$$E_{edge}=\frac{J^{ah}}{\tilde{r}}L^{ah}r. \tag{15}$$

Using Eq. (10), Eq. (15) can be written as

$$E_{edge}=\left(\frac{N}{N-n_h}\right)^{1/2}E_{edge}^{\text{model}}, \tag{16}$$

or in an expanded form,

$$E_{edge}=\frac{1}{2}\left(\frac{N}{N-n_h}\right)^{1/2}\sum J_{ij}^{ah}[s_i(1-s_j)+s_j(1-s_i)]. \tag{17}$$

C. Programming and analysis

To create and recover holes in the membrane up to an equilibrium point, we use the Metropolis algorithm in the Monte Carlo simulation. The mass of a hole is zero, but the mass of the system or number of particles is conserved through the renormalization of Eq. (6). Although the occupation of sites changes as the simulation evolves, detailed balance is satisfied because each configuration of pores has a uniquely defined energy. This energy does not depend upon the path followed to reach it. The transition probability between a given initial and final configuration will also be unique and reversible. If we choose an occupied site with the same probability than an empty site, that is, we select particles or holes according to their surface distribution; the acceptance rule will be given by

$$\text{acc}(i\rightarrow f)=\min\{1,\exp[-(\tilde{H}_f-\tilde{H}_i)/k_BT]\}, \tag{18}$$

in order to respect detailed balance. This acceptance rule is the usual one for a Monte Carlo simulation in the canonical ensemble. Finally, periodic boundary conditions are considered on the hexagonal lattice.

The approach is highly efficient and large systems can be studied, up to 10^7 particles. However, systems of 10^4 particles, which correspond to small vesicles, are normally sufficient. Usually within 1000 samplings per site, the equilibrium state is easily reached.

IV. RESULTS

The types of membranes we study can be grouped in three main categories: saturated lipid bilayers (typical), unsaturated lipid bilayers, and long chain diblock copolymer bilayers. Membranes with unsaturated lipids may be found in biological systems. The long tail diblock copolymers, however, were synthesized by Bermudez *et al.*, and then used to build vesicle shape polymersomes [34]. In Table I the important parameters for our study are grouped. Those values are the total number of unsaturated bonds, the compressibility K, the membrane core thickness $2h_t$, the permeability, the critical tension for rupture τ^*, and the corresponding stretching $\Delta a_m^*/a_m$. Values for lipid membranes were taken from Olbrich *et al.* [8] and Rawicz *et al.* [19]. The unsaturated lipid membranes differ from the typical membranes in the stiffness of their tails, while the diblock copolymers simply have longer tails.

In summary (details appear in the following subsections), our strategy was to first use the above parameters to determine γ the tail rigidity by looking at the effect it has on the critical rupture tension. K being known, every choice of γ sets also the value of the apparent hydrophobicity σ through Eq. (8). Experimentally, K seems independent of tail structure for most lipids [19], but the rupture kinetics are not and this, we assume, is due mainly to changes in rigidity or γ. The compressibility of long tail copolymers is different from the usual 243 mN/m mainly because the head group is different, and not because of the tail length [34]. We will focus our attention mainly on the typical bilayers.

Once γ and hence σ are set, we study the scenario of rupture through an ''equilibrium'' phase diagram that looks at the different qualitative changes in the distribution of pores as a function of stretching for temperatures around k_BT_{room}. This corresponds to slow (quasistatic) stretching rates that keep the membrane in a state of equilibrium with respect to the applied stress. In the case of a higher rate of expansion, larger stretches and therefore tensions will be needed to break the membrane [29,30]. Because we are considering thermally activated processes, higher temperatures in this model are equivalent to weaker interactions. To study the reversibility of membrane lysis, hysteresis curves were constructed to compare the number of holes and their distribution as we first stretch the membrane to rupture, and then let it relax to zero tension. This study revealed that the rupture transition is first order at room temperature, with a strong hysteresis. The fractal dimensions of stable pores were computed at different temperature as a measure of their entropy and shape. As a prelude, we look at system size dependence.

A. System size dependence

To simplify the discussion, we assume that the correct tail rigidity has been obtained. In reality, the numerical value of the tail rigidity depends somewhat on system size.

Bilayer membranes can form vesicles of a variety of shapes. In nature, they are normally present as spherical vesicles of radii between 1 and 10 μm [11–13]. For a given relative stretch $\Delta a_m/a_m$, the surface energy per particle does not depend on the size of the lattice. The line energy scales as the length of pore edge or the sum of the square root of the surfaces of the individual pores. System size may affect the kinetics because of the changes in pore size distribution and the fact that pore size distribution does not scale with system size.

As shown in Fig. 2, stretching to rupture almost stabilizes to about 3.9% for systems larger than 10^4 particles. For smaller systems, we observe a significant increase. As expected, this plateau is mainly due to the increase in the

TABLE I. Compressibility and other known physical parameters of the different types of membranes studied. These parameters are the total number of *cis*-unsaturated bonds in the lipid tails (''*uns.*''), the compressibility K, the thickness of the tails $2h_t$, the permeability P, the critical tension for rupture τ^*, and corresponding area stretching $\Delta a_m^*/a_m$. Values for typical (i.e., with none or only one unsaturated bond) and unsaturated lipids are from Olbrich *et al.* [8] and Rawicz *et al.* [19], whereas the values for long tail diblock copolymers are taken from Bermudez *et al.* [34].

Membrane	*Uns.*	K (mN/m)	$2h_t$ (nm)	P (μm/s)	τ^* (mN/m)	$\Delta a_m^*/a_m$ (%)
Typical (average)						
	0, 1	243±24	3.0±0,1	35±7	9±2	3,9±0,9 [a]
Unsaturated lipids						
SLPC:0/2[a]	2	243±24	3.0±0,1	49±6	4,9±1,6	2,0±0,5 [g]
DLPC:2/2[b]	4	243±24	3.0±0,1	91±24	5,1±1,0	2,1±0,4 [g]
LPC:3/3[c]	6	243±24	3.0±0,1	146±24	3,1±1,0	1,2±0,4 [g]
Long tail copolymers						
OE7[d]	0	102±10	8±1		21±3 [g]	21±2
OB9[e]	0	102±10	11±1		28±4 [g]	28±3
OB19[f]	0	102±10	21±1		40±5 [g]	40±4

[a]SLPC: 0/2 = 1-stearoyl-2-linoleoyl$_{cis\ at\ 9,12}$-phosphatidylcholine.
[b]DLPC: 2/2 = dilinoleoyl$_{both\ cis\ at\ 9,12}$-phosphatidylcholine.
[c]DLPC: 3/3 = dilinoleoyl$_{both\ cis\ at\ 9,12,15}$-phosphatidylcholine.
[d]OE7 = ethylenoxide$_{40}$-ethylethylene$_{37}$.
[e]OB9 = ethylenoxide$_{50}$-butadiene$_{55}$.
[f]OB19 = ethyleneoxide$_{150}$-butadiene$_{250}$.
[g]Values obtained using Eq. (2), and strains or stresses to rupture from quoted articles.

number of pores at rupture, which raises the line energy (see Fig. 3). Furthermore, entropy increases for larger systems, which favors earlier rupture. These plots are averages with a standard deviation of ten runs. It is an interesting and open question to know if multiple pore rupture is observed in biological membranes. It must be noted that the number of sites in our simulations corresponds to half the number of particles, since we are dealing with bilayer membranes. For what follows, we shall work on a lattice of 30 301 sites (60 602 lipids). This corresponds to a total membrane area of 18 μm^2 ($a_0 \approx 0.6$ nm^2 for phospholipids). For a spherical vesicle, this means a radius of 1.5 μm, the size of a small natural biological cell.

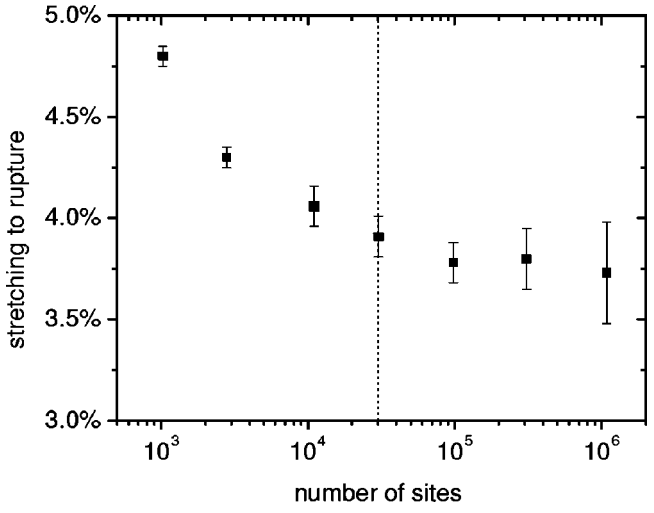

FIG. 2. The dependence of the degree of stretching on the size of the membrane for rupture at room temperature. The number of sites is half the number of particles since we are working with a bilayer. This value stabilizes at area expansions near 4% for systems larger than 10^4 sites. The dashed line indicates the size of the network used in the rest of the simulations.

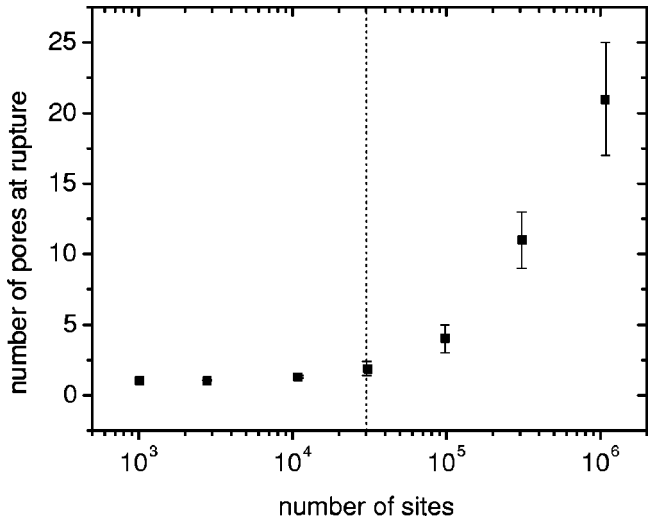

FIG. 3. The average number of stable pores in the system when it ruptures at room temperature. The relation is linear (exponential on this log scale). The dashed line indicates the size of the network used in the rest of the simulations.

B. The rigidity and hydrophobicity of lipid tails

Depending on the rigidity of the tails of a lipid, more or less water may penetrate the membrane under stretching. For unsaturated lipids, one would expect higher rigidities, since the tails are stiffer. Furthermore, if the tails are rigid, the membrane is also more permeable [19]. In this case, the apparent hydrophobicity of the membrane is lower, since the difference in energy for the lipid inside and outside the membrane is smaller. For small variations of these parameters, we can see from Eq. (7) that a saturated and an unsaturated membrane made out of the same lipid group should have comparable compressibilities. This was verified experimentally by Rawicz *et al.* [19] in their investigation of the effects of lipid unsaturation on membrane elasticity. This group has found that unsaturation has no effect on compressibility. Nevertheless, unsaturation is still an important issue for membrane rupture, as unsaturated lipids are less flexible than saturated ones. Olbrich *et al.* [8] have discovered that rupture tension was only affected for bilayers made with lipids of two or more alternating *cis*-double bonds (C═C—C═C) in one or both chains. The three degrees of unsaturation that we study are as shown in Table I: lipids with one tail having two alternating *cis*-double bonds (one pair), both tails having two alternating *cis*-double bonds (two pairs), and both tails with three alternating *cis*-double bonds (four pairs). All these unsaturated lipids also have 18 carbon atoms in each tail. For the long polymers, the line energy is directly proportional to the length of the lipid tails. It is therefore natural to expect higher tensions at rupture for longer chains. Membrane rupture of diblock copolymers membranes will also be studied.

To obtain γ and therefore σ, of the different membranes, we fit the tail rigidity to have the appropriate stretching to rupture. For typical lipid bilayer membranes, we need a rigidity of $\gamma = 8 \pm 1$ to have rupture at 3.9% (see Fig. 4). From Eq. (7), this corresponds to a hydrophobicity of 7.6.

The plateau near 2% stretching in Fig. 4 for large γ's may seem abnormal at first sight. And just before zero tension rupture, there is even a slight increase in the stretching to rupture. This effect is related to the criterion that defines rupture. Zero tension rupture means that the lipids are so stiff and the membrane so permeable that stability is not assured. Just before this critical rigidity, the membrane is still not very stable, since the line energy per lipid rapidly decreases with stretching. This weak interaction between lipids raises the entropy of the system. For high rigidities, this gain in entropy will make the rupture scenario more comparable to a melting phenomenon than a pore creation relaxation. Since we have lost the ideal scenario of rupture that favors relaxation as opposed to the creation of line energy, rupture in terms of a few stable pores is more difficult to achieve. The definition of rupture will be discussed in more detail in the following section.

Nevertheless, this plateau seems consistent with experimental observations. Unsaturated lipids with two and four total unsaturated bonds both have a stretching to rupture near 2% (see Fig. 4). This therefore means that even though they have the same stretching to rupture does not mean that they have the same tail rigidity. In fact, they should not.

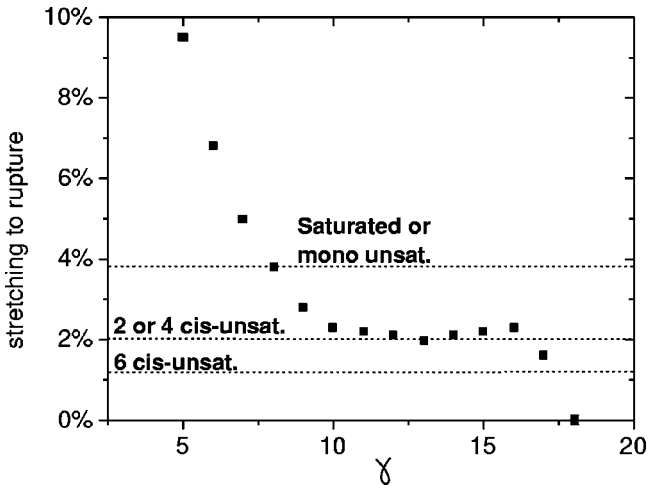

FIG. 4. The degree of stretching for rupture at room temperature for different tail rigidities for membranes with compressibility of 243 mN/m and membrane core thickness of 3.0 nm (see Table I). The dashed lines are the known area expansions at rupture for membranes with different degrees of unsaturation.

For typical membranes, the apparent hydrophobicity σ is about five times smaller than the approximated value for σ_{pure} (see Table II). This leads to a line energy of 2.4×10^{-8} mN, well within the experimentally measured range of $1-4 \times 10^{-8}$ mN. For highly unsaturated lipids, this ratio can be as high as ten if we suppose that the pure hydrophobicity has not changed significantly. It would be wrong, however, to say that 80% of the membrane is flooded. This apparent hydrophobicity may also take into account other repulsive energies, such as the head-head repulsion. The noticeable difference between the pure and the apparent hydrophobicities indicates that the membrane permeability is not a negligible effect.

Graphics similar to Fig. 4 were used to obtain the tail rigidity of the diblock copolymers studied by Bermudez *et al.* [34]. The tail rigidity of OE7 and OB8 is comparable to the rigidity of a typical lipid tail. However, for OB19, which has a much longer tail (see Table I) γ is considerably higher. It may be that for very long polymers tail entanglements make the tails appear more rigid [34,35].

In the following sections, we focus on *typical* biological membranes. So γ is set equal to 8.

C. Phase diagram

A phase diagram was constructed to study the behavior of the membrane under variations of the temperature and the surface area (i.e., under stretching). We show the phase diagram in Fig. 5 for a ''typical'' membrane (see Table I). The most striking feature is a ''first-order transition'' line to a ruptured state. When at a given temperature, the membrane is stretched, one observes in the neighborhood of a specific stretch an abrupt increase in the relaxation which we call *rupture*. This occurs through the formation of a few massive stable pores. The line shown in Fig. 5 corresponds to the point of abrupt relaxation as the tension is increased. Below this line the nature of the membrane evolves gradually with

TABLE II. Tail rigidity and apparent hydrophobicity of the different lipids studied. The estimated value for pure hydrophobicity is also given as a reference.

Membrane	Name	*Uns.*	γ	σ (mN/m)	σ_{pure} (mN/m)
Typical	(average)	0, 1	8.0 ± 1.0	7.6	40
Unsaturated	SLPC:0/2	2	13.0 ± 3.0	4.7	≈40
Lipids	DLPC:2/2	4	13.0 ± 3.0	4.7	≈40
	DLPC:3/3	6	17.5 ± 0.5	3.8	≈40
Long tail	OE7	0	7.3 ± 1.0	3.4	
Copolymers	OB9	0	8.6 ± 1.0	2.9	
	OB19	0	13.0 ± 1.0	2.0	

temperature T. At low T, including around T_{room}, there is what we call a *stable* state. The relaxation in this regime is small, with occasionally a few protopores (see Sec. IV E). As the temperature is raised the number and the size of the protopores keep increasing. The pores become numerous, but are still short lived, and of size not larger than ten particles or so.

At temperatures below and near T_{room}, rupture is very sharp. We go directly from a state of high tension where less than 20% of the membrane is relaxed to an almost fully relaxed system (80% and more). At higher temperatures, there are a larger number of pores present in the membrane at low stretches, but they do not aggregate till the tension reaches the rupture tension.

The rupture line first decreases with temperature till $1.6T_{room}$ then rises again. Entropy appears to favor a high density of dispersed pores. It takes then an increased tension to force the aggregation of the pores and trigger the full relaxation of the membrane. This leads to the rise in the rupture tension. Finally, the rupture line ends near $T=2.8T_{room}$, but it is no longer a first-order transition line. At that temperature the membrane loses stability; *stable* pores are created without any tension applied. The reduced line energy λ/k_BT falls below the critical value required to assure membrane stability. Shillcock and Boal [27] vary λ in their tethered beads model. They find a critical value of $\lambda^* b/k_BT=1.66$ at constant zero tension, where b is the average vertex separation in their model (At T_{room}, this means a critical line energy of about 0.9×10^{-11} J/m). We work at constant area and, in our model, we calculate hole-lipid interactions and the total line energy is given by $J^{ah}L^{ah}$ [see Eq. (15)], where J_{ij}^{ah} is the hole-lipid interaction defined in Eq. (13). The effective line tension depends on pore distribution. With our thermally activated model the behavior observed near $2.8T_{room}$ can be viewed as behavior near T_{room} with a line energy reduced by the factor 2.8. Using the distribution of pores in Fig. 7(c), one can find an effective line energy per site of $\approx1.1J^{ah}$ (small pores dominate the distribution) [36], or a critical line energy per unit length of about 0.94×10^{-11} J/m. Interestingly, our lattice model and Shillcock and Boal's bond flipping model have consistent views on stability. Mechanically, the membrane may fail earlier so we label the region around $T=2.8T_{room}$ as *unstable*.

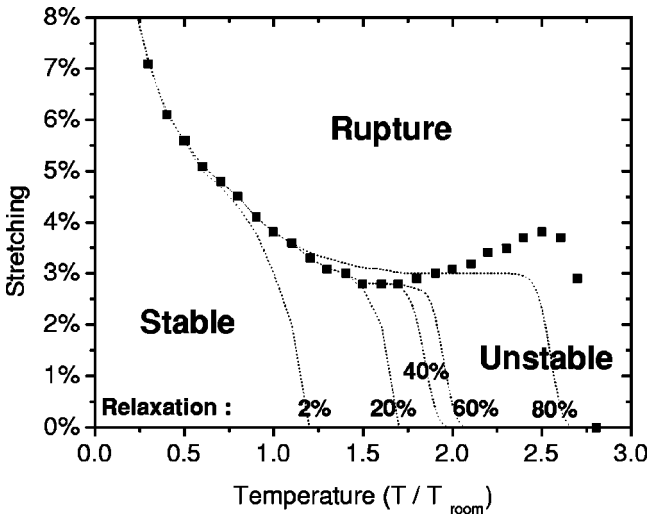

FIG. 5. Phase diagram predicted by the model for a ''typical'' bilayer (see Table I) showing the degree of relaxation in the membrane as a function of stretching and temperature. The full square dots indicate the rupture first-order transition line. The dashed lines are the curves of constant relative relaxation.

At room temperature, the presence of a regime offering 2%–20% unstable pore surface, or small nonstable pores, called protopores, have experimentally been observed at room temperature [4]. In the following three sections, we look at different properties of the membrane under tension that give a clearer picture of the rupture kinetics.

D. Hysteresis

To show that indeed rupture is of ''first-order,'' samples were put through a full cycle of expansion and compression. This is done again in a quasistatic process, i.e., at each step the system is allowed to relax. We follow, as the strain was varied, the variations in the stress [Fig. 6(a)], the relative pore area (a measure of the relaxation)[Fig. 6(b)], and the total number of pores (a measure of pore interaction and coalescence) [Fig. 6(c)].

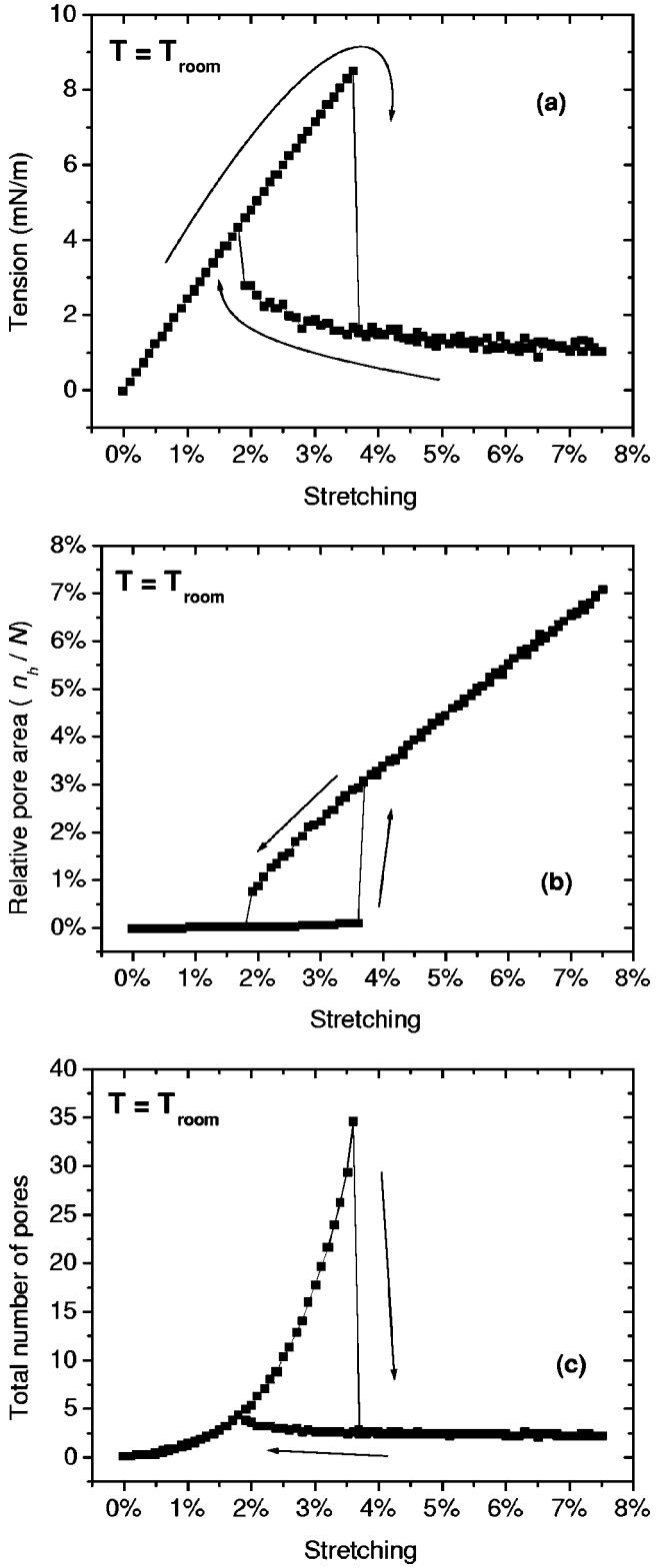

FIG. 6. Hysteresis of different quantities upon stretching at $T=T_{room}$: (a) the tension τ; (b) the relative area occupied by pores which is equal to the number of pore sites divided by the total number of sites; (c) the total number of pores. Room temperature systems behave similarly to high temperature systems at low tensions by having a considerable quantity of protopores present in the membrane. The rupture scenario is, however, similar to that of lower temperature systems.

Hysteresis effects are found to be very strong at low temperature. Rupture and healing occur through nucleation of one pore. At high temperature, hysteresis is reduced and there are many more pores present, below and above rupture. At T_{room}, the case illustrated in Figs. 6, behavior is similar to the high temperature situation below rupture, but comparable to the low temperature case above rupture. A considerable number of pores are present in the membrane at first, but after rupture, only a small number of large nonfluctuating pores remain. This is clearly observable in Fig. 6(c) as the rapid rise in the number of pores which precedes the collapse at rupture. The tension at collapse defines the T_{room} point on the rupture line.

E. Pore size distribution

To further illustrate the difference in pore distribution below and above rupture, we compare the distribution of pore sizes for membranes with 2% and 6% strain. We do this at the three temperatures T_{room}, $2T_{room}$, and $3T_{room}$ to illustrate the change in structure of the membrane with increasing temperature [see Figs. 7(a)–(c)]. The distributions are typical snap shots of the membrane as the Monte Carlo simulation evolves. For the stable membranes shown, we see in Figs. 7(a) and 7(b), the sharp drop in the number of small pores above rupture. A large pore creates less line energy than a protopore for the same gain in surface energy, so is energetically favored. For unstable membranes, the appearance of larger pores in the system does not reduce the number of smaller ones [Fig. 7(c)]. The small pores, present at zero tension at $3T_{room}$ are stable due to the contribution of entropy to the free energy. This illustrates from another perspective the instability of the membrane at $3T_{room}$.

F. Pore shape

At different temperatures for a stretching of 3% (just before rupture), we insert into the membrane a hole at the origin. After the pore is fully opened and stable, we compute its fractal dimension d_f from the scaling relationship between the pore area A and its perimeter l ($A=A(0)l^{d_f}$, where A_0 is a proportionality factor).

From the results plotted in Fig. 8, we clearly see that d_f decreases as the temperature is raised. This is caused by increased irregularities along the edge of the pore. At $T=2.8T_{room}$, where rupture occurs spontaneously at zero tension, one would expect the scaling relationship applicable to a self-avoiding ring [27]. In such geometries, the area of the pore should scale as $A=A_0l^{3/2}$. For this case, our model gives $d_f=1{,}54\pm0{,}10$ in agreement with this argument.

V. CONCLUSION

Bilayer membranes are an intrinsic part of all living species. With the rapid development of biotechnology, membranes can now be artificially created, and thereafter even modified to form vesicles of controlled size and properties. Rupture kinetics play an integral part in the modifications of those vesicles and in their applications such as in drug delivery.

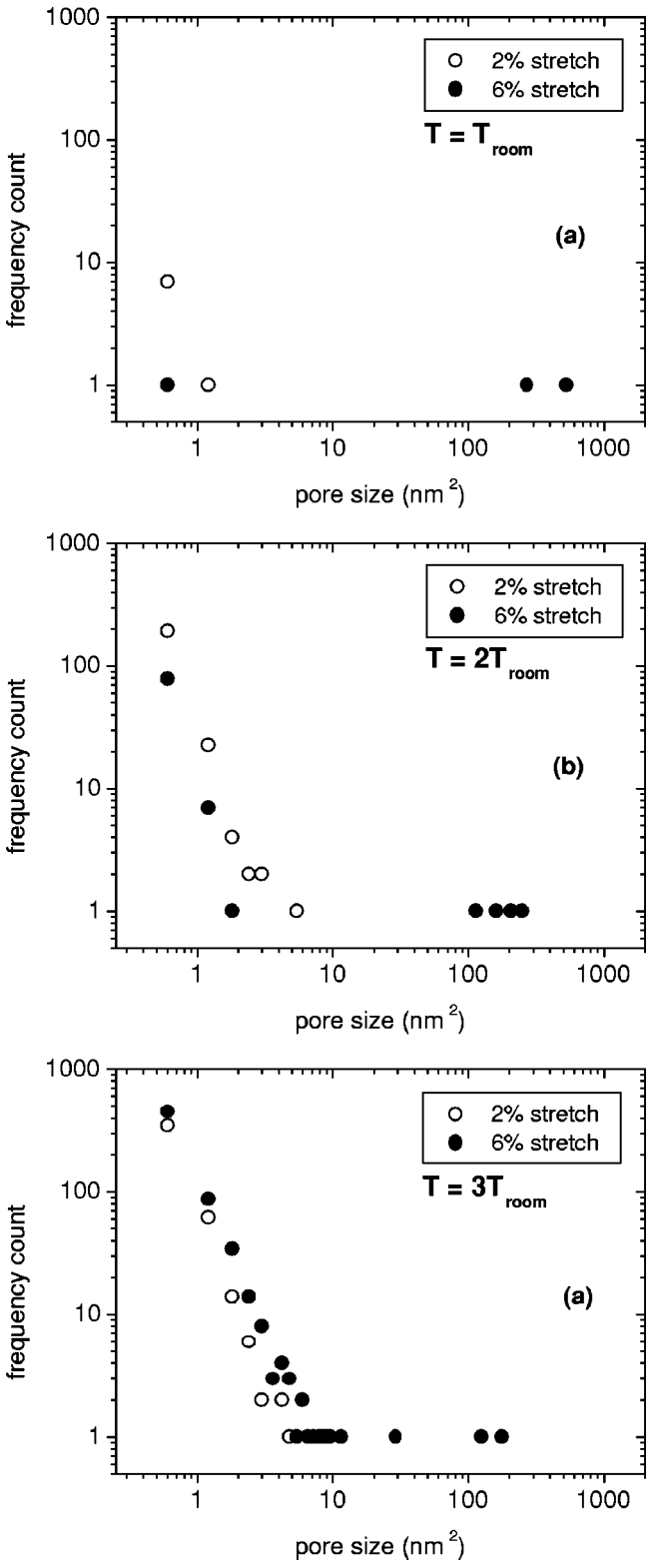

FIG. 7. Distribution of pores at three temperatures (a) $T=T_{room}$, (b) $T=2T_{room}$, and (c) $T=3T_{room}$, below and above the rupture point in a lattice of 30 301 sites (each site ≈ 0.6 nm^2). With increasing temperature, the number of small pores increases and a larger number remain in the system after rupture. At $T=3T_{room}$, above the instability point of $2.8T_{room}$, there is little structural difference between a 2% and 6% stretched membrane except for the larger size of the pores.

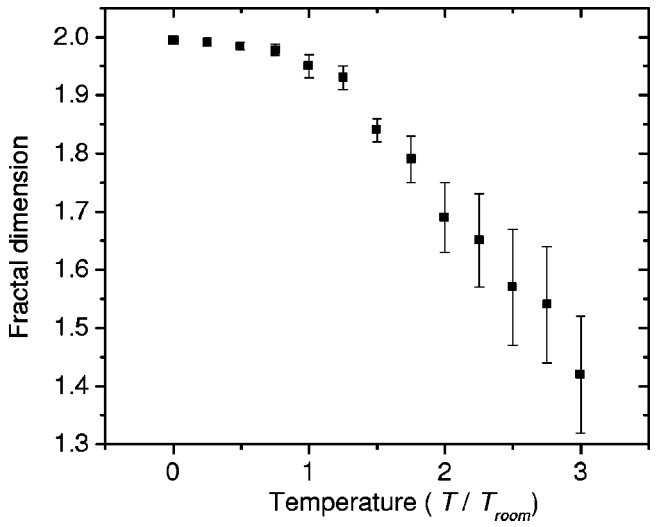

FIG. 8. The fractal dimension of a pore in a stretched membrane. This quantity is a measure of the regularity of the shape of the pore and its edge. As the temperature is increased, the pore becomes irregular and spreads over a larger membrane surface.

In spite of their complex molecular structure, lipid bilayer membranes offer an ideal model system, as hydrophobicity is responsible for both the line energy and the bulk compressibility (for extension). We have developed the model for the rupture of a membrane held together by hydrophobic forces, which includes the nucleation and growth of pores. Our minimal model can be used to reproduce current results on saturated and unsaturated PC lipid bilayers and thicker artificial bilayers made of diblock copolymers. We have introduced a quantity called the rigidity of the tails γ that permits to study the effect of saturation of the lipid tails on the structural properties of the bilayer. Interestingly an increase in rigidity produces a decrease in apparent hydrophobicity, since K is nearly constant for a given class of lipids. This may mean an increase in permeability. The model requires little computer time allowing the handling of real size vesicles. Entropic and nucleation effects are included naturally.

The structural integrity of a lipid bilayer is considerably affected by its composition; biological membrane structure can be fairly complex. Different types of lipids, cholesterols, and proteins play an important role in determining membrane stability. The model has the potential of handling these inclusions.

ACKNOWLEDGMENTS

The authors wish to thank Michael Wortis, James Polson, David Boal, Dennis Discher, and Martin Zuckermann for many stimulating discussions. The work has been funded by the Natural Sciences and Engineering Research Council (Canada).

[1] D.S. Dimitrov and R.K. Jain, Biochim. Biophys. Acta **779**, 437 (1984).
[2] W. Harbich and W. Helfrich, Z. Naturforsch. A **34A**, 1063 (1979).
[3] I.G. Abidor, V.B. Arakelyan, L.V. Chernomodik, Y.A. Chizmadzhev, V.F. Patushenko, and M.R. Tarasevich, Bioelectrochem. Bioenerg. **6**, 37 (1979).
[4] D. Needham, and R.M. Hochmuth, Biophys. J. **55**, 1001 (1989).
[5] C. Wilhelm, M. Winterhalter, U. Zimmermann, and R. Benz, Biophys. J. **64**, 121 (1993).
[6] M. Winterhalter, Colloids Surf., A **149**, 161 (1999).
[7] S.Y. Ho and G.S. Mittal, Crit. Rev. Biotechnol. **16**, 349 (1996).
[8] K. Olbrich, W. Rawicz, D. Needham, and E. Evans, Biophys. J. **79**, 321 (2000).
[9] D.G. Hunter and B.J. Frisken, Biophys. J. **74**, 2996 (1998).
[10] A. Ertel, A.G. Marangoni, J. Marsh, F.R. Hallett, and J.M. Wood, Biophys. J. **64**, 426 (1993).
[11] B.L.-S. Mui, P.R. Cullis, E.A. Evans, and T.D. Madden, Biophys. J. **64**, 443 (1993).
[12] C. Taupin, M. Dvolaitzky, and C. Sauterey, Biochemistry **14**, 4771 (1975).
[13] J.S. Remy, A. Kichler, V. Mordvinov, F. Schuber, and J.P. Behr, Proc. Natl. Acad. Sci. U.S.A. **92**, 1744 (1995).
[14] F.D. Ledley, Hum. Gene Ther. **6**, 1129 (1995).
[15] N.M. Correa and Z.A. Schelly, Langmuir **14**, 5802 (1998).
[16] D. Boal, *Mechanics of the Cell* (Cambridge University Press, Cambridge, 2001).
[17] J. Wolfe, M.F. Dowgert, and P.L. Steponkus, J. Membr. Biol. **86**, 127 (1985).
[18] E.A. Evans and D. Needham, J. Phys. Chem. **91**, 4219 (1987).
[19] W. Rawicz, K.C. Olbrich, T. McIntosh, D. Needham, and E. Evans, Biophys. J. **79**, 328 (2000).
[20] Z. Zhou and B. Joós, Phys. Rev. B **56**, 2997 (1997).
[21] J. Akinlaja and F. Sachs, Biophys. J. **75**, 247 (1998).
[22] D.V. Zhelev and D. Needham, Biochim. Biophys. Acta **1147**, 89 (1993).
[23] O. Sandre, L. Moreaux, and F. Brochard-Wyart, Proc. Natl. Acad. Sci. U.S.A. **96**, 10 591 (1996).
[24] J.D. Litster, Phys. Lett. **53A**, 193 (1975).
[25] A. Barnett and J.C. Weaver, Bioelectrochem. Bioenerg. **25**, 163 (1991).
[26] S.A. Freeman, M.A. Wang, and J.C. Weaver, Biophys. J. **67**, 42 (1994).
[27] J.C. Shillcock and D.H. Boal, Biophys. J. **71**, 317 (1996).
[28] R.R. Netz and M. Schick, Phys. Rev. E **53**, 3875 (1996).
[29] E. Evans and F. Ludwig, J. Phys.: Condens. Matter **12**, 315 (2000).
[30] E. Evans and V. Heinrich (unpublished).
[31] J. N. Israelachvili, *Intermolecular and Surface Forces: With Applications to Colloidal and Biological Systems* (Academic Press, London, 1985), Chap. 16.
[32] M. Wortis and E. Evans, Phys. Canada **53**, 281 (1997).
[33] E. Evans and W. Rawicz, Phys. Rev. Lett. **64**, 2094 (1990).
[34] H. Bermudez, A.K. Brannan, D.A. Hammer, F.S. Bates, and D.E. Discher, Macromolecules **35**, 8203 (2002).
[35] B.M. Discher, Y.-Y. Won, D.S. Ege, J.C.-M Lee, F.S. Bates, D.E. Discher, and D.A. Hammer, Science **284**, 1143 (1999).
[36] The two limiting values of L^{ah} are a monovacancy $L^{ah}=1$ per site, for a straight segment of pore, $L^{ah}=2$. For small pores with all its n_i sites neighboring a lipid site, $L^{ah}=6+2n_i$ and the smallest perimeter is equal to $6+2(n_i-1)$ sites.